Cell Reports

Article

Virtual flying experience changes neural responses to seeing wings

Graphical abstract

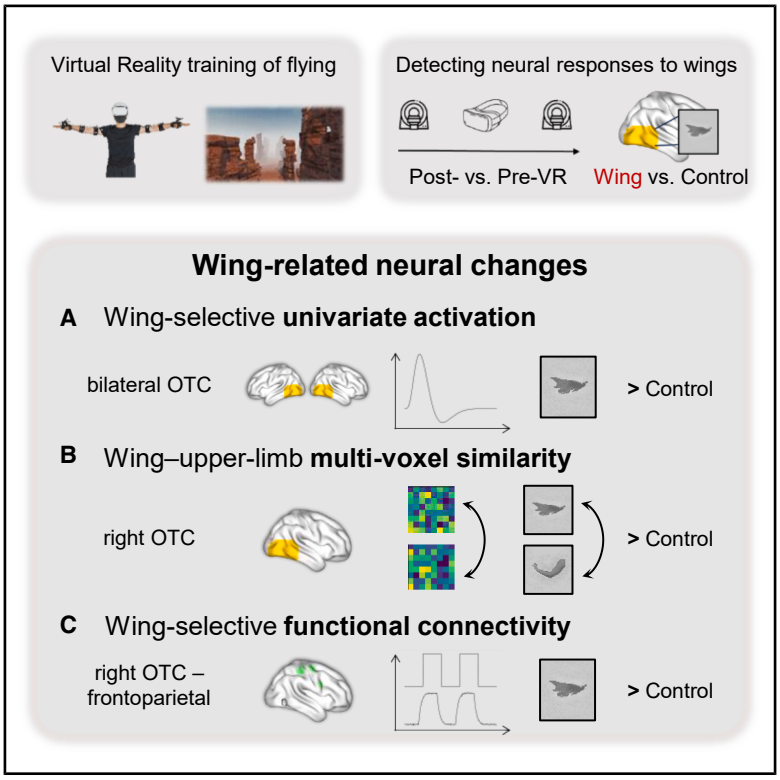

Highlights

- VR enables embodiment of illusionary wings through upper-limb control
- Occipitotemporal cortex shows wing-enhanced activation and limb-like representation
- Wing images evoke enhanced occipitotemporal-frontoparietal functional coupling
- Human visual system incorporates wings as effectors via functional-semantic coding

Authors

Ziyi Xiong, Yiyang Cai, Xiaosha Wang, Kunlin Wei, Yanchao Bi

Correspondence

wei.kunlin@pku.edu.cn (K.W.), ybi@pku.edu.cn (Y.B.)

In brief

How does the human brain adapt to evolutionarily atypical experiences? By employing a virtual reality flying training paradigm, Xiong et al. demonstrate that the human brain incorporates illusionary wings into its body representation system via functional-semantic coding, transcending mere visual familiarity and low-level sensorimotor congruence.

Xiong et al., 2026, Cell Reports ■■, 117320
■■, 2026
https://doi.org/10.1016/j.celrep.2026.117320

CellPress

Cell Reports

CellPress
OPEN ACCESS

Article

Virtual flying experience changes neural responses to seeing wings

Ziyi Xiong,[1,6] Yiyang Cai,[2,3,6] Xiaosha Wang,[2,3,4,1] Kunlin Wei,[2,3,*] and Yanchao Bi[2,3,4,5,1,7,*]
[1]State Key Laboratory of Cognitive Neuroscience and Learning & IDG/McGovern Institute for Brain Research, Beijing Normal University, Beijing 100875, China
[2]School of Psychological and Cognitive Sciences and Beijing Key Laboratory of Behavior and Mental Health, Peking University, Beijing 100871, China
[3]Key Laboratory of Machine Perception (Ministry of Education), Peking University, Beijing 100871, China
[4]IDG/McGovern Institute for Brain Research, Peking University, Beijing 100871, China
[5]Institute for Artificial Intelligence, Peking University, Beijing 100871, China
[6]These authors contributed equally
[7]Lead contact
*Correspondence: wei.kunlin@pku.edu.cn (K.W.), ybi@pku.edu.cn (Y.B.)
https://doi.org/10.1016/j.celrep.2026.117320

SUMMARY

The human brain visually processes body parts in the occipitotemporal cortex (OTC), a category-selective organization proposed to reflect evolutionary salience. Using virtual reality (VR), we investigated how the OTC adapts to artificial body parts—virtual wings—that transcend evolutionary constraints. Participants underwent a week of VR training (four sessions), learning to control virtual wings via upper-limb movements with simulated visual feedback of flight. Comparing pre- and post-VR neural responses to wing images shows changes in the OTC, characterized by (1) increased bilateral wing-selective activation, (2) enhanced multi-voxel representational similarity between wings and upper limbs in the right OTC, and (3) strengthened task-dependent functional coupling (psychophysiological interaction) of wing stimuli between the right OTC and frontoparietal high-level somatosensory and motor associate regions. These findings show that the OTC incorporates illusionary effectors into body representations that transcend lower-level sensorimotor congruence, highlighting its role in the abstract, functional-semantic coding of visual inputs.

INTRODUCTION

The remarkable plasticity of the human brain enables continuous adaptation to sensorimotor changes and lifelong learning, facilitating the acquisition of robust knowledge.[1] Under natural conditions, this neural "plasticity" operates within evolutionarily constrained brain networks, processing sensorimotor experiences where signals from multiple sensorimotor modalities—visual, proprioceptive, and motor—are tightly coupled. For example, upper-limb movements generate synchronous visual, proprioceptive, and motor signals that reinforce the neural representations of the involved body effectors. Modern virtual reality (VR) technologies can disrupt this fundamental sensorimotor congruence by creating illusionary, artificial visuomotor associations—such as visual feedback that systematically contradicts actual body movements or presents entirely non-biological morphologies.[2,3] Artificial sensorimotor experiences in VR often deviate from the expected congruence of the biological body, effectively "tricking" the human brain into incorporating non-human body effectors. This paradigm raises critical neuroscientific questions: how does the human brain respond to these evolutionarily unprecedented experiences? Does the human brain incorporate artificial effectors as actual body parts? The predictions for these questions rely on how the brain typically processes body part information and the principles underlying its learning-induced changes.

The occipitotemporal cortex (OTC), particularly its lateral subregion (the lateral occipitotemporal cortex [LOTC]) encompassing the extrastriate body area (EBA), has exhibited robust and selective responses to visually presented bodies and body parts across numerous studies.[4–8] As part of the ventral visual pathway, the OTC is canonically believed to represent bodies and body parts primarily based on visual inputs.[9,10] Evidence has also been reported regarding the OTC's representational content that challenges a purely visual account. For example, body selectivity in this region has been observed when congenitally blind individuals perceive body-part shapes via auditory inputs in sensory-substitution paradigms[11]; responses to body-effector images (e.g., upper limbs in healthy subjects or lower limbs in individuals with congenital dysplasia) and manipulable object (tool) images are found to overlap in the LOTC, reflecting the functional extensions of body effectors[12–14]; and functionally related body effectors (e.g., hands and feet for motor execution; eyes and mouths for social communication) exhibit multi-voxel representational similarities.[15] While these findings have been interpreted as supporting an abstract,

Please cite this article in press as: Xiong et al., Virtual flying experience changes neural responses to seeing wings, Cell Reports (2026), https://doi.org/10.1016/j.celrep.2026.117320

"functional-semantic" representation in the OTC, they can alternatively be accommodated by associations within the visual modality (e.g., visual co-occurrence, shared visual features) and/or between visual and other sensorimotor modalities (e.g., haptic, proprioceptive, and motor) supported by neural connectivity,[12,16] without appealing to more abstract semantics. Specifically, the OTC has been reported to functionally[16–18] and structurally[19] connect with regions encompassing widespread frontoparietal somatosensory and motor associate regions, which support functions such as motor execution, movement planning, motor imagery, and action observation.[20,21]

How do the OTC's responses to visual stimuli "plastically" change through learning? Specific types of training paradigms sharpen the OTC's neural representations: individuals with extensive Pokémon experience show enhanced neural sensitivity to Pokémon images in the OTC, characterized by stronger univariate activation and greater multi-voxel representational dissimilarity from other object categories, such as animals[22]; prolonged tool use[23] or prosthetic use[24,25] leads to increased activation and representational divergence between the trained devices and upper limbs. That is, the use of tools or prosthetics did not "embody" these objects as body parts but instead led to more specific categorical representations. These training paradigms entail multiple information types—visual input, multimodal associations, and functional-semantic knowledge. It is not clear which factor(s) govern the observed learning-induced neural changes (i.e., activation strength, multi-voxel pattern, and/or connectivity) associated with the learned stimuli.

In VR, illusionary experiences can be tailored to deviate from evolutionarily normative sensorimotor experiences. We developed a paradigm in which participants learned to "embody" wings that could be controlled for flying in a virtual environment. Their upper-limb movements, captured by motion-tracking devices, were translated into corresponding wing movements that drove egocentric visual scene motion during simulated flight, which was vividly presented in a head-mounted display (Figure 1A). Through a four-session, seven-day training regimen, participants learned to control the virtual wings with simulated aerodynamics to fly skillfully in a virtual space, thereby establishing an atypical sensorimotor congruence between their upper-limb movements and the resulting visual consequences. Does this artificial experience change the OTC's response to viewing wings, and if so, how (Figure 1B; see Figure 1C for an overview of the analytical pipeline)? If the OTC were shaped solely by the visual experience, we would expect minimal change in its response profile, given that direct visual exposure to the wings during egocentric VR flight is limited, or we would expect a sharpening of the wing-selective response (i.e., stronger univariate activation and/or enhanced multi-voxel representational distinctiveness for the specific wing exemplar used in training). Similarly, if the OTC were shaped solely by motor experience constrained by existing human body effectors, no changes would be expected either, as upper-limb movements map onto upper limbs in biological reality rather than onto wings. If, however, the OTC is sensitive to an abstract, functional-semantic interpretation of wings, then the recently established sensorimotor congruence—interpreting upper-limb movements as the act of flying with wings—should result in changed responses to wings at the object categorical level, leading to wing neural representations that move closer to the body-effector (upper-limb) space. We also examined whether the observed functional changes within the local OTC were associated with its connectivity changes with frontoparietal somatosensory and motor associate regions, to elucidate network-level and connectivity-sensitive plastic properties.

RESULTS

Participants (n = 25) were recruited to undergo four sessions of VR training between two functional magnetic resonance imaging (fMRI) scans performed 7 days apart. During VR training, they wore a head-mounted display (HMD) and were equipped with reflective markers placed on their upper limbs, which were captured by a motion-tracking system to record real-time movements. The recorded kinematics were transmitted synchronously to drive virtual wing-flapping animations within the HMD, enabling interactive wing control (via upper-limb movements) during gamified VR tasks. Each VR training session began with a five-minute familiarization phase during which participants performed a posture-imitation task and an airball task. These tasks were designed to facilitate adaptation to the sensorimotor congruence between upper-limb movements and visual wing feedback. Subsequently, they completed a 25-min flying training phase comprising four specific tasks: single flap, maximum-velocity flight, altitude maintenance, and ring navigation (Figure 1A). A simplified aerodynamic model was implemented to simulate lift generation during downward wing-flaps and drag during upward flaps. Participants learned to optimize flight efficiency by mastering the simulated aerodynamics: fully extending the wings during downward strokes to maximize lift, while contracting the wings during upward strokes to minimize drag. At the conclusion of each session, participants performed a final ring-navigation task, with the hit rate (percentage of successful ring passes) recorded as a behavioral index of proficiency. Additionally, they rated their perceived sense of agency (SoA) over the virtual wings using a seven-point Likert scale adapted from established VR illusion studies.[26,27]

We conducted fMRI experiments both before and after the VR training. Data from a *picture-viewing experiment* and a *video-viewing experiment* were utilized for the primary analyses, while data from a separate *motor localizer experiment* were used to define motor regions of interest (ROIs). In behavioral data analyses, we examined whether participants' performance, including flying proficiency and the SoA over the virtual wings, improved across the training sessions. In the fMRI analyses, we first identified cortical regions where the activation strengths to wing images were specifically modulated by VR training (fMRI univariate analysis). To further characterize the neural response changes and test the functional-semantic hypothesis of wing embodiment, we examined the informational content using multi-voxel pattern analysis (MVPA; fMRI representational pattern analysis). We additionally performed functional connectivity (FC) analyses using data from the *picture-viewing experiment* and the *video-viewing experiment* to assess changes in wing-sensitive inter-regional coupling (fMRI functional connectivity analysis).

Please cite this article in press as: Xiong et al., Virtual flying experience changes neural responses to seeing wings, Cell Reports (2026), https://doi.org/10.1016/j.celrep.2026.117320

CellPress
OPEN ACCESS

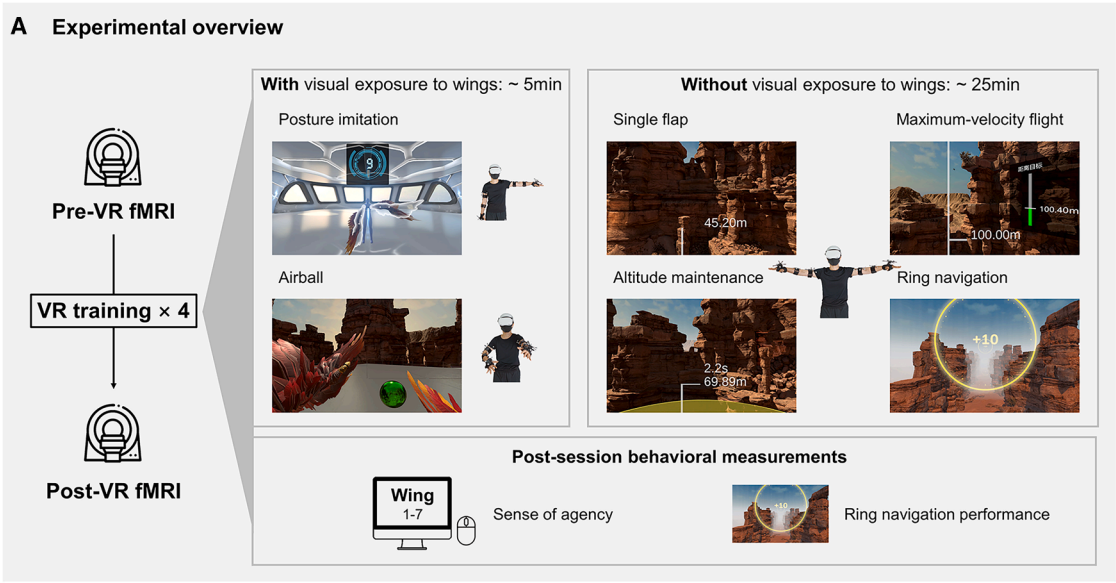

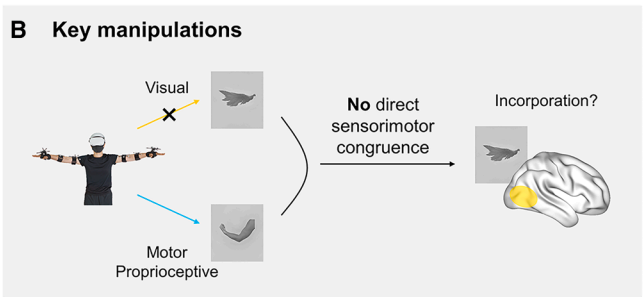

C Overview of results

Neural changes tested	Figure index
Wing-univariate strength	Figure 2
Wing-representational pattern	Figure 3
Wing-functional connectivity	Figure 4

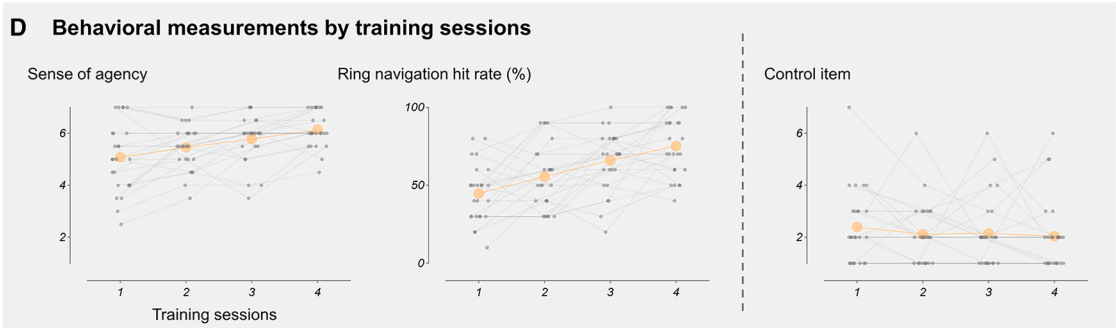

Figure 1. Experimental design

(A) Experimental timeline showing four VR training sessions interspersed with two fMRI scanning sessions (pre- and post-fMRI). During VR training, participants performed wing-related movements with their upper limbs while receiving corresponding visual feedback of scene changes driven by virtual aerodynamics. Training phases: the initial phase (first 5 min per session) included posture imitation (copying outlines on a virtual mirror) and an airball task (wing flapping to deflect balloons; wings visible). The main phase involved flight training with four tasks (25 min per session) with the wings invisible. After each training session, participants rated their sense of agency over the virtual wings and took an additional ring navigation test.

(B) The key experimental design involves probing virtual usage of wings without direct sensorimotor congruence.

(C) We investigate three types of changes to wings or the VR setting.

(D) Post-session assessment results. Subjective sense of agency ratings, ring navigation performance (hit rate through 10 rings), and control item are illustrated. Orange dots represent the group mean, and gray dots represent individual participants (n = 25).

Behavioral results: VR training enhances flying proficiency and sense of agency over virtual wings

We compared behavioral performance across the four training sessions (Figure 1D). Participants exhibited significant improvements in both flying proficiency and their SoA over the virtual wings. From the first to the fourth session, the mean hit rate in the ring-navigation task increased from 44.8% (±18.5%) to 75.2% (±19.2%), and the SoA score rose from 5.08 (±1.34)

Please cite this article in press as: Xiong et al., Virtual flying experience changes neural responses to seeing wings, Cell Reports (2026), https://doi.org/10.1016/j.celrep.2026.117320

to 6.14 (±0.69). These gains were statistically confirmed by one-way repeated-measures analyses of variance (ANOVAs; hit rate: $F_{[3,72]} = 16.69$, $p < .001$, $\eta_p^2 = 0.41$; SoA: Greenhouse-Geisser corrected $F_{[2.14,\ 51.44]} = 12.64$, $p < .001$, $\eta_p^2 = 0.35$). A control item was included in the questionnaire to monitor potential task compliance and suggestibility effects. While the control item showed non-significant change across sessions ($F_{[3,72]} = 0.44$, $p = .727$), a significant interaction between item type (SoA vs. control) and training (from session 1 to session 4) was observed (Greenhouse-Geisser corrected $F_{[2.19,\ 52.64]} = 4.99$, $p = .009$, $\eta_p^2 = 0.17$), confirming a selective increase in SoA over wings.

Picture-viewing experiment fMRI univariate analysis: VR training induces wing-selective activation changes in the bilateral occipitotemporal cortex

To assess neural response changes to wing images, we compared the neural activation of wings between post- and pre-VR sessions. We used the mean activation across all other experimental categories (including human body parts, animal body parts, and man-made objects) as a baseline (Figure 2A). This approach controlled for potential global fMRI signal amplitude differences across scanning sessions—which could otherwise be misinterpreted as training-specific effects—while minimizing object-category-specific biases. Specifically, these changes were quantified through a 2 × 2 repeated-measures ANOVA with VR training session (post, pre) and object type (wing, non-wing) as within-subject factors.

Enhanced wing-selective responses in bilateral OTC

Whole-brain VR training (post, pre) × object type (wing, non-wing) random-effect (RFX) interactions were observed in bilateral OTC regions (Figure 2A, upper panel; voxel-level $p < .001$, cluster-level family-wise error [FWE] corrected $p < .05$): left OTC (peak Montreal Neurological Institute [MNI] coordinate: [−52 −66 −4], peak $t_{[24]} = 5.02$, 129 voxels) and right OTC (peak MNI coordinate: [48 −64 −6], peak $t_{[24]} = 5.02$, 93 voxels). The interactions were driven by an increased wing activation relative to other conditions in the post-VR scan (see Figure 2A for simple effects of VR training and Figure S1A for raw activations). The reversed direction yielded null results even under a more lenient threshold of voxel-level $p < .005$ and cluster-level FWE-corrected $p < .05$. These clusters (hereafter "OTC_{wing}") were situated in the anterior and ventral portions of the anatomical LOTC (Harvard-Oxford Atlas, hereafter "$LOTC_{anat}$"). They also lay anterior and ventral to the classic body-selective EBA parcel defined in a previous work.[28] We observed that 16 of 129 voxels in the left OTC_{wing} and all 93 voxels in the right OTC_{wing} overlapped with the EBA parcel (see Figure S2 for spatial overlaps).

Laterality of wing-selective response changes

We quantified potential hemispheric differences in the wing-selective univariate changes using Laterality Indices (*LI*s). *LI*s were derived based on the VR training (post, pre) × object type (wing, non-wing) interaction using the *LI* toolbox[29] (see STAR Methods). Specifically, we examined lateralization within the $LOTC_{anat}$ mask (Figure 2B, left panel) and the entire occipital lobe (as implemented in the toolbox). By definition, *LI* values range from −1 (completely right-lateralized) to 1 (completely left-lateralized), with the [−.2, .2] interval indicating bilaterality.[30,31] The calculated *LI*s for both the $LOTC_{anat}$ (.14) and the entire occipital lobe (.09) fell within the bilateral range, suggesting bilateral VR-training-induced effects.

No differential response changes across wing types

The functional-semantic embodiment hypothesis posits the formation of an abstract, categorical representation of wings, rather than one tied to specific visual exemplars encountered during VR training. Alternatively, it is possible that the minimal residual visual experience of wings might contribute to the univariate changes observed in the OTC.[22] The latter possibility would predict that visually exposed wings ("VR-self") would exhibit greater univariate changes than non-exposed wings ("bird"). We directly tested these competing predictions using a repeated-measures ANOVA with training session (pre vs. post) and wing category (VR-self vs. bird) as factors. The analysis revealed no interaction effect in OTC_{wing} ($F_{[1,24]} = 0.08$, $p = .777$), which was further supported by a Bayesian repeated-measures ANOVA ($BF_{incl} = 0.30$), providing moderate evidence in favor of the null hypothesis (H_0) of no interaction. These results suggest that the observed change is not specific to the wing images seen in the training.

Replication of wing-selective changes in classic anatomical LOTC and body-part-sensitive EBA

The wing-selective univariate changes were then more specifically tested in LOTC and EBA, regions implicated in multimodal body-part perception and functional extension (e.g., tool perception and upper-limb-tool overlap).[5,11,13,32–34] ROI-level analyses were performed using two independent sets of masks: the anatomically defined $LOTC_{anat}$ and the functionally defined $EBA_{neurosynth}$ derived from a *Neurosynth* meta-analysis of body-processing studies (Figure 2B, left panel).[35] Significant VR training (post, pre) × object type (wing, non-wing) interactions were consistently replicated across ROI definitions in both hemispheres (all $F_{[1,24]} > 5.50$, $p < .028$, $\eta_p^2 > 0.19$; Figure 2B, right panel; see Table S1 for detailed statistics). We also examined potential differences between wing types through VR training (post, pre) × object type (VR-self, bird) interaction, which yielded non-significant results across all regions (all $F_{[1,24]} < 0.23$, $p > .637$; $BF_{incl} < 0.31$), providing moderate evidence in favor of H_0. See Figure S1B for condition-specific activations.

Overall, these findings demonstrate that the "flying with wings" VR training selectively enhances neural responses to wings in bilateral OTC regions.

Picture-viewing experiment fMRI representational pattern analysis: VR training enhances neural representational similarity between wings and upper limbs in the right occipitotemporal cortex

Next, to investigate how the neural representations of wings are modulated by VR training, we evaluated voxel-wise representational patterns of wings relative to other conditions using support vector machine (SVM) classifiers in MVPA. We defined the condition-pair representational similarity as "100% minus pairwise classification accuracy" in each scanning session. Note that we do not focus on the similarity between conditions at one time point (i.e., within pre- or post-VR scanning), as this similarity might arise from shared low-level visual features (e.g., elongated

Please cite this article in press as: Xiong et al., Virtual flying experience changes neural responses to seeing wings, Cell Reports (2026), https://doi.org/10.1016/j.celrep.2026.117320

CellPress
OPEN ACCESS

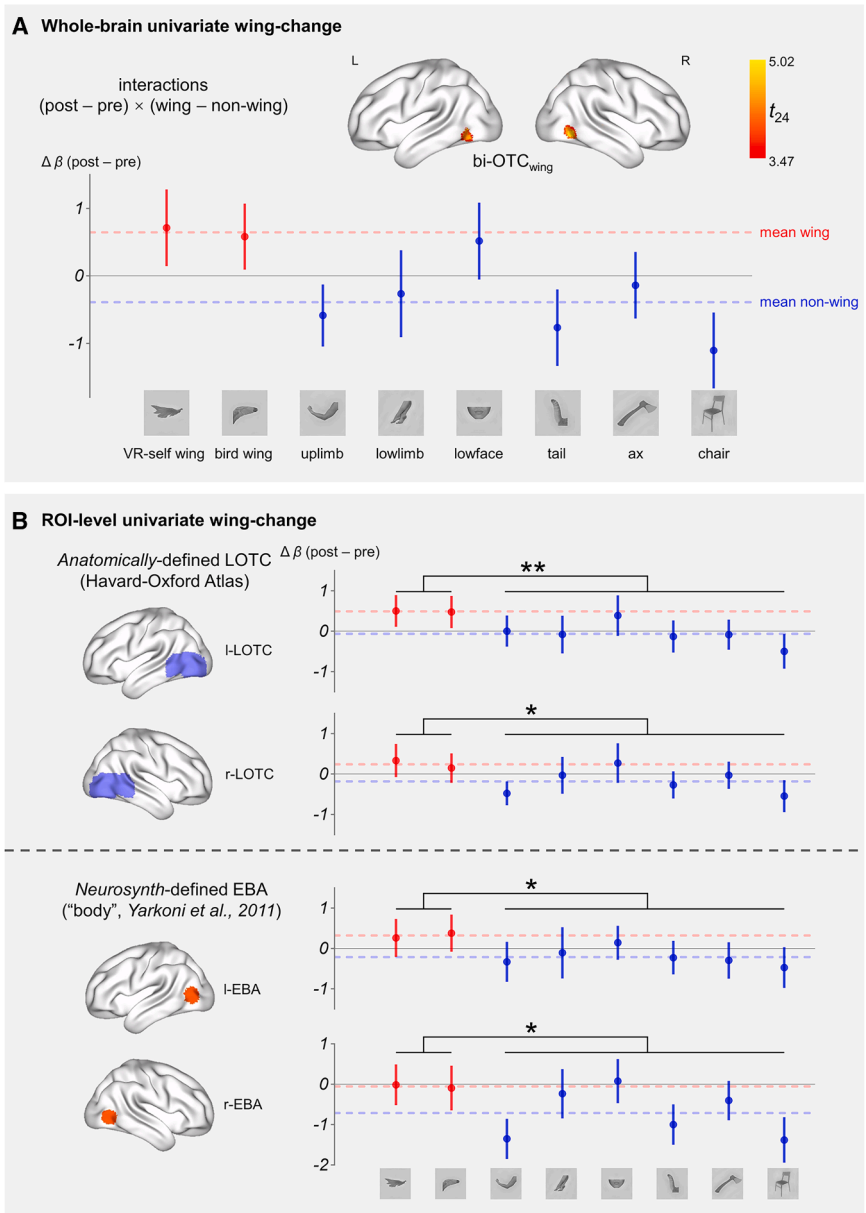

Figure 2. Wing univariate functional profile changes following VR training

(A) Whole-brain analysis showing the VR training (post- vs. pre-VR) × object type (wing vs. non-wing) interaction in bilateral occipitotemporal cortex (OTC, voxel-level $p < .001$, cluster-level FWE corrected $p < .05$).

(B) ROI-level analysis confirmed the effects across different OTC region definitions (anatomical and meta-analysis-based). Bar plots show simple effects (post vs. pre) for each condition. Error bars: SEM ($n = 25$). L/R: left/right. $^{**}p < .01$, $^{*}p < .05$ for interaction effects in repeated measures ANOVA. See also Figure S1, Table S1.

shape),[36] which were not intentionally controlled for. The key focus of MVPA is the change in representational similarity from pre- to post-VR training.

Guided by the functional-semantic embodiment hypothesis (see Introduction), we tested whether VR training leads to a specific shift in neural representation whereby wings become more similar to upper limbs than to other object conditions. This hypothesis was examined through a 2 × 2 ANOVA with VR training session (post, pre) and object-pair type (wing-upper-limb, wing-others) as within-subject factors. We first performed ROI-level MVPA in the independently defined LOTC and EBA regions, followed by exploratory whole-brain searchlight analyses.[37] Note that the MVPA results in OTC$_{wing}$ identified in the univariate analyses above (Figure S3) were consistent with results in the independently defined ROIs reported in the following sections.

Please cite this article in press as: Xiong et al., Virtual flying experience changes neural responses to seeing wings, Cell Reports (2026), https://doi.org/10.1016/j.celrep.2026.117320

Increased wing-upper-limb representational similarity in right OTC regions

The right $LOTC_{anat}$ and $EBA_{neurosynth}$ exhibited significant VR training session (post, pre) × object-pair type (wing-upper-limb, wing-others) interaction effects (right $LOTC_{anat}$: $F_{[1,24]} = 18.63$, $p < .001$, $\eta_p^2 = 0.44$; right $EBA_{neurosynth}$: $F_{[1,24]} = 8.84$, $p = .007$, $\eta_p^2 = 0.27$). Post-hoc simple effect analyses revealed that the similarity between wings and upper limbs significantly increased following VR training (post vs. pre; r-$LOTC_{anat}$: $t_{[24]} = 3.29$, two-tailed $p = .003$, Cohen's $d = 0.66$; r-$EBA_{neurosynth}$: $t_{[24]} = 2.68$, two-tailed $p = .013$, Cohen's $d = 0.54$), whereas the similarity between wings and the average of other conditions did not change significantly (post vs. pre, right $LOTC_{anat}$: $t_{[24]} = -0.27$, two-tailed $p = .793$, $BF_{10} = 0.22$, moderate evidence in favor of H_0 of no difference; right $EBA_{neurosynth}$: $t_{[24]} = -0.91$, two-tailed $p = .374$, $BF_{10} = 0.31$, moderate evidence in favor of H_0). Notably, the interactions between VR training session (post, pre) and object-pair type (wing-upper-limb, wing-others) were non-significant in the left $LOTC_{anat}$ or $EBA_{neurosynth}$ ($F_{[1,24]} < 2.55$, $p > .123$; see Table S2 for detailed statistics). These null effects were further characterized by Bayesian statistics (left $LOTC_{anat}$: $BF_{incl} = 1.10$, anecdotal evidence in favor of the alternative hypothesis [H_1] of an interaction effect; left $EBA_{neurosynth}$: $BF_{incl} = 0.32$, moderate evidence in favor of H_0 of no interaction; Figure 3A).

Searchlight analysis identifies increased wing-upper-limb similarity in the right OTC

Whole-brain searchlight[37] (8-mm-radius spheres) RFX MVPA of the VR training (post, pre) × object-pair type (wing-upper-limb, wing-others) interaction peaked at the right OTC region at the threshold of voxel-level $p < .001$, which was the largest cluster (peak MNI coordinate: [44 −56 −2], peak $t_{[24]} = 4.98$, 146 voxels; Figure 3B), despite the fact that it did not survive the cluster-level correction. The interaction reflected the direction of relatively more similar neural representations between wings and upper limbs, compared to between wings and other objects in the post-VR scan. This cluster lay on the anterior and ventral portion of the right $LOTC_{anat}$, and 101 voxels of it overlapped with the right EBA parcel defined by Julian et al.,[28] which converged well with ROI-level results (Figure S2). The reversed direction yielded null results even under a more lenient threshold of voxel-level $p < .005$ and cluster-level FWE-corrected $p < .05$.

Laterality of wing-upper-limb pattern similarity change

The above whole-brain searchlight analysis identified the largest cluster in the right OTC and not in the left, and the ROI-level analyses revealed a significant wing-upper-limb similarity change in the right, but not the left hemisphere. We formally assessed the potential lateralization using the *LI*. Following the same procedure as for the univariate laterality analysis, we computed *LI*s within the anatomical LOTC ($LOTC_{anat}$) and the entire occipital lobe. The results consistently showed that the VR training (post, pre) × object-pair type (wing-upper-limb, wing-others) interaction was strongly right-lateralized ($LI = -.68$ in $LOTC_{anat}$ and $LI = -.71$ in the entire occipital lobe).

No differential change across wing types in representational similarity

Similar to the fMRI univariate findings above, we tested here whether VR-self-wing and bird-wing representations exhibited differential patterns of change in right OTC. To isolate the selective changes within the wing-upper-limb pair while controlling for baseline similarity differences, we calculated a "wing-upper-limb similarity index" by subtracting the average similarity between wing and other conditions from the wing-upper-limb similarity. Changes between different types of wings were not significant, as revealed by the VR training (post, pre) × wing type (VR-self-wing-index, bird-wing-index) interaction effects (right $LOTC_{anat}$: $F_{[1,24]} = 0.93$, $p = .345$, $BF_{incl} = 0.52$, anecdotal evidence in favor of H_0 of no interaction effect; right $EBA_{neurosynth}$: $F_{[1,24]} = 0.25$, $p = .622$, $BF_{incl} = 0.27$, moderate evidence in favor of H_0).

Upper-limb representational specificity

We considered whether the wing-upper-limb similarity was driven by a generalized change in upper-limb representation, a question we treat as open. One theoretical possibility is that the enhanced representation of wings in the OTC "compresses" the representational space of upper limbs, resulting in greater similarity between upper limb and *all* non-wing object conditions. This is similar to the cortical reorganization effect observed in the primary motor cortex when adding a "sixth" finger following motor training compresses the representational space of the existing fingers.[38] Another non-mutually exclusive possibility is that the effect was strongest for the wing-upper-limb pair, indicating a more targeted functional embodiment.

Direct post vs. pre-VR comparison of upper-limb-other (non-wing) similarities revealed null results in right $LOTC_{anat}$ ($t_{[24]} = 1.43$, two-tailed $p = .167$) and right $EBA_{neurosynth}$ ($t_{[24]} = 1.03$, two-tailed $p = .315$). Bayesian statistics revealed anecdotal evidence in favor of the H_0 of no difference ($BF_{10} = 0.52$ and $BF_{10} = 0.34$, respectively). We also performed the VR training session (post, pre) × object-pair type (wing-upper-limb, upper-limb-others) ANOVA to test whether wing-upper-limb similarity change exceeded the general upper-limb change. Right $LOTC_{anat}$ showed significant interaction effect ($F_{[1,24]} = 5.25$, $p = .031$, $\eta_p^2 = 0.18$), and right $EBA_{neurosynth}$ showed a similar trend ($F_{[1,24]} = 2.56$, $p = .122$). These results (Figure 3A) suggest that VR training specifically changes the relationship between wings and upper limbs rather than inducing a generalized change in the limb-related representational space.

Together, these results demonstrate that VR training induces a selective enhancement of wing-upper-limb representational similarity in the body-processing regions of the right OTC.

fMRI functional connectivity analysis: VR training strengthens wing-selective functional coupling between the right OTC and high-level somatosensory and motor regions

To investigate how VR training modulates functional connectivity patterns associated with wing processing, we applied two complementary task-state functional connectivity (FC) analyses in two fMRI experiments. Using the fMRI *picture-viewing experiment* data, we first performed generalized psychophysiological interaction (gPPI) analyses examining VR-training-induced connectivity changes related to wings through the VR training (post, pre) × object type (wing, non-wing) interaction. The gPPI investigates how a specific task condition modulates the coupling between brain regions beyond intrinsic connectivity.[39,40] To rule out non-specific attentional effects that might enhance connectivity

Please cite this article in press as: Xiong et al., Virtual flying experience changes neural responses to seeing wings, Cell Reports (2026), https://doi.org/10.1016/j.celrep.2026.117320

CellPress
OPEN ACCESS

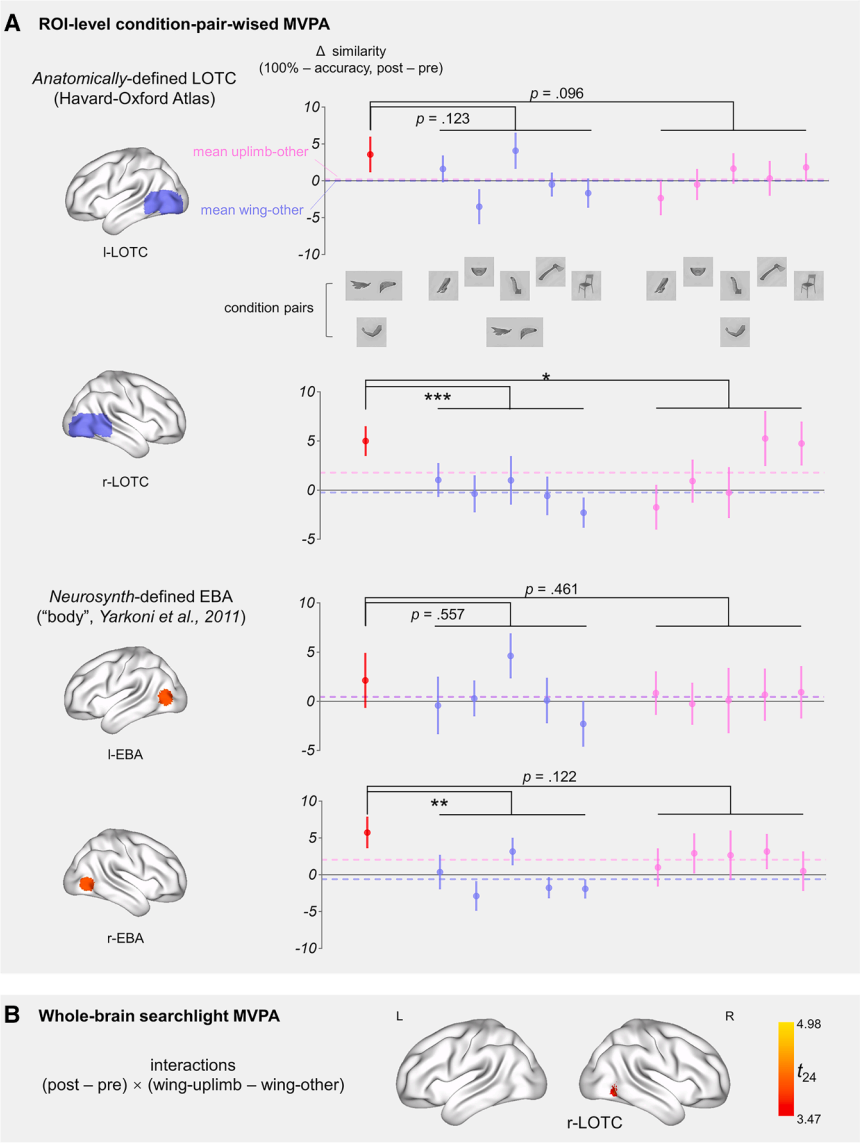

Figure 3. Wing representational similarity functional profile changes following VR training

(A) ROI-level MVPA: increased wing-upper-limb similarity compared with other objects in right OTC regions.

(B) Whole-brain searchlight MVPA identified right OTC (thresholded at voxel-level $p < .001$, cluster size >100 voxels, for visualization purposes). Bar plots show simple effects (post vs. pre) for each condition pair. Error bars: SEM ($n = 25$). ***$p < .001$, **$p < .01$, and *$p < .05$ for interaction effects in repeated measures ANOVA. See also Figure S3, Table S2.

for all VR-experienced stimuli, we conducted complementary task-state FC analyses during the egocentric VR flying *video-viewing experiment*. We tested two primary predictions: (1) the connectivity between OTC and sensorimotor regions—high-level and primary somatosensory and motor regions—is strengthened post-training selectively for wing stimuli (via gPPI), and (2) these effects are absent in the task-state FC analyses during egocentric VR-flying-video viewing (reflecting sensitivity to VR setting in general). To ensure signal homogeneity, all connectivity analyses employed the OTC_{wing} peak voxels (4-mm-radius spheres) as seeds.[41,42] We also replicated the results using the full OTC_{wing} clusters.

Increased wing-selective gPPI connectivity between the right OTC_{wing} and high-level somatosensory and motor associate regions

A significant VR training (post, pre) × object type (wing, non-wing) interaction was observed in the gPPI connectivity between the right OTC_{wing} spherical seed and high-level somatosensory and motor associate regions ($F_{[1,24]} = 13.76$, $p = .001$, $\eta_p^2 = 0.36$). Post-hoc simple effect analyses revealed that functional coupling significantly increased for wing conditions following VR training (post vs. pre, $t_{[24]} = 2.67$, two-tailed $p = .014$, Cohen's $d = 0.53$), whereas no such change was observed for non-wing conditions (post vs. pre, $t_{[24]} = 1.25$, two-tailed $p = .224$;

Please cite this article in press as: Xiong et al., Virtual flying experience changes neural responses to seeing wings, Cell Reports (2026), https://doi.org/10.1016/j.celrep.2026.117320

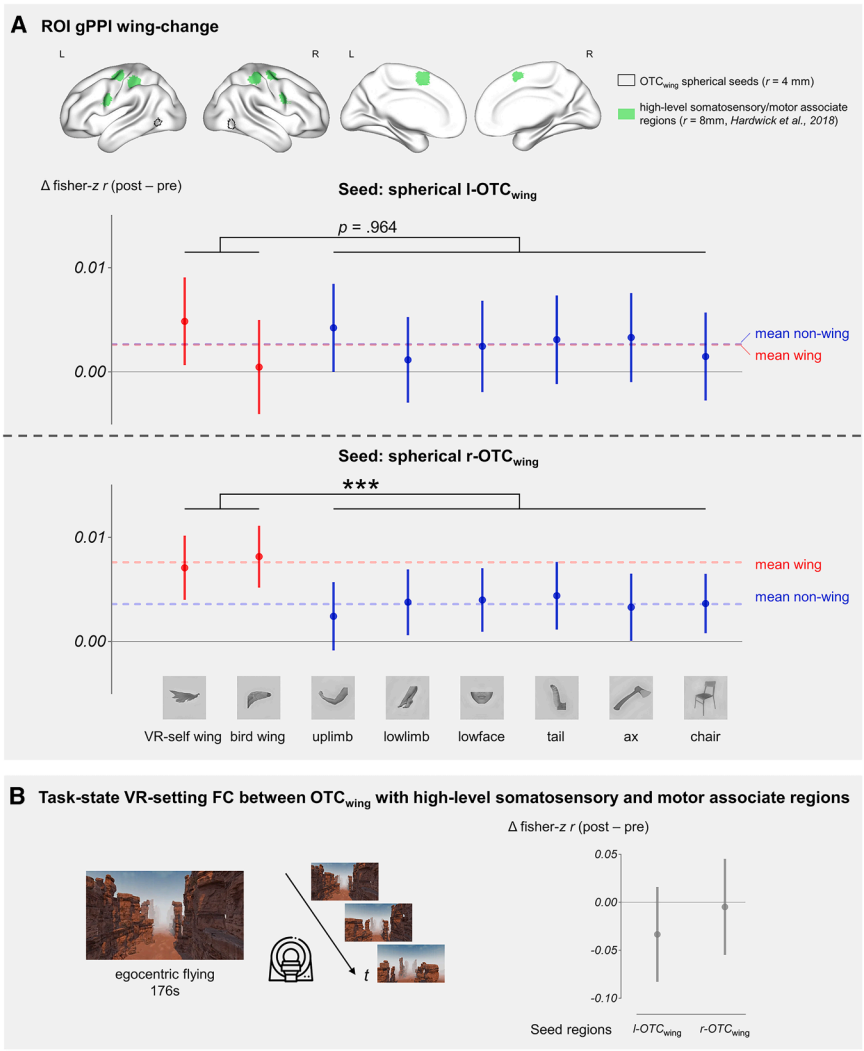

Figure 4. Wing functional connectivity changes following VR training

(A) ROI-level gPPI: enhanced connectivity of right OTC$_{wing}$ with high-level somatosensory and motor associate regions during wing processing.

(B) No task-state functional connectivity was observed between the OTC$_{wing}$ and high-level somatosensory and motor associate regions during video viewing. Bar plots show PPI simple effects (post vs. pre) for each condition or task FC changes (post vs. pre). Error bars: SEM (n = 25). ***p < .001 for interaction effects in repeated measures ANOVA. See also Figure S4, Table S3.

BF_{10} = 0.42, anecdotal evidence in favor of H_0). Furthermore, a direct comparison of VR training (post, pre) × wing types (VR-self-wing vs. bird-wing) yielded non-significant interaction with the training session ($F_{[1,24]}$ = 0.29, p = .594), with Bayesian analysis providing moderate evidence for the null hypothesis (BF_{incl} = 0.33). The wing-selective connectivity of the left OTC$_{wing}$ spherical seed with high-level somatosensory and motor regions revealed null results ($F_{[1,24]}$ < 0.01, p = .964, BF_{10} = 0.21), providing moderate evidence in favor of H_0 of no training effect in the left hemisphere (see Figure 4A for condition-specific changes). To ensure the robustness of our findings, we performed the gPPI analysis using the full OTC$_{wing}$ as seeds. ROI-level analyses replicated the interaction effects (right OTC$_{wing}$ cluster with high-level somatosensory and motor associate regions: $F_{[1,24]}$ = 13.54, p = .001, η_p^2 = 0.36; left OTC$_{wing}$ cluster: $F_{[1,24]}$ = 0.04, p = .845; BF_{10} = 0.28, moderate evidence in favor of H_0). The raw connectivity strengths are detailed in Figure S4A.

One possible interpretation is that the apparent increase in connectivity might reflect a shift from negative (anti-correlated) values toward approximately zero, which could actually indicate a reduction in anti-correlation rather than a genuine strengthening of functional coupling. To examine this possibility, for the connectivity between the right OTC$_{wing}$ spherical seed and high-level somatosensory and motor associate regions, we compared the connectivity values against zero (representing the null state of no coupling) for wing and non-wing conditions in both pre- and post-VR sessions. In the pre-VR session, neither wing nor non-wing connectivity differed significantly from zero (M_{wing} = −0.001, $t_{[24]}$ = −0.63, one-tailed p = .267; BF_{-0} = 0.37, anecdotal evidence in favor of H_0 of not

Please cite this article in press as: Xiong et al., Virtual flying experience changes neural responses to seeing wings, Cell Reports (2026), https://doi.org/10.1016/j.celrep.2026.117320

below zero; $M_{non\text{-}wing} = -2.54 \times 10^{-4}$; one-sample t tests, $t_{[24]} = -0.12$, one-tailed $p = .452$, $BF_{-0} = 0.23$, moderate evidence in favor of H_0). In contrast, in the post-VR session, wing-related connectivity was significantly greater than zero ($M_{wing} = 0.006$, $t_{[24]} = 2.54$, one-tailed $p = .009$, Cohen's $d = 0.51$), while non-wing connectivity remained not significantly different from zero ($M_{non\text{-}wing} = 0.003$, $t_{[24]} = 1.24$, one-tailed $p = .113$, $BF_{+0} = 0.73$, anecdotal evidence in favor of H_0 of not above zero). These findings suggest that the observed effect reflects a genuine enhancement of wing-selective connectivity rather than a mere attenuation of anti-correlation.

Laterality of wing-selective gPPI connectivity changes

The aforementioned gPPI analyses revealed that VR training significantly altered connectivity between the right OTC_{wing} seed and high-level somatosensory and motor associate regions, whereas no such changes were observed for the left OTC_{wing} seed. This hemispheric difference was statistically confirmed by a significant three-way within-subject ANOVA, which revealed a significant hemisphere (left, right) $\times$ VR training (post, pre) $\times$ object type (wing, non-wing) interaction ($F_{[1,24]} = 6.97$, $p = .014$, $\eta_p^2 = 0.23$). That is, the observed connectivity change was stronger in the right hemisphere.

No change in wing-selective gPPI connectivity between the OTC_{wing} and primary effector-specific somatosensory and motor regions

To further explore whether the training-induced changes in connectivity extended to more primary, effector-specific somatosensory and motor regions (S1/M1), we also examined the gPPI connectivity of the left and right OTC_{wing} regions with S1/M1 upper-limb-specific regions. Non-significant interaction effects were found in these analyses (all $F_{[1,24]} < 0.16$, $p > .697$). Bayesian ANOVAs consistently provided moderate evidence in favor of H_0 of no change in connectivity ($BF_{incl} < 0.31$; see Figure S4B for raw connectivity patterns and see Table S3 for detailed statistics). Given these null findings, we refrained from further interpretation of connectivity changes between the OTC and S1/M1 upper-limb-specific regions.

No changes in OTC-sensorimotor region connectivity during general VR-video viewing

A major alternative explanation is that the connectivity increase reflects general VR effects like heightened attention or episodic recall for the trained stimulus, rather than wing-selective, functional-semantic change. To rule out this possibility, we next investigated task-state FC patterns when participants viewed an egocentric flying video filmed in the VR training by an independent participant (author Y.C.; VR *video-viewing experiment*). We observed non-significant changes in connectivity strength between OTC_{wing} and high-level somatosensory and motor associate regions (post vs. pre; left OTC_{wing} sphere with high-level somatosensory and motor associate regions: $t_{[24]} = -0.67$, two-tailed $p = .505$; right OTC_{wing} sphere: $t_{[24]} = -0.10$, two-tailed $p = .925$; Figure 4B; see Figure S4C for session-specific connectivity). Bayesian paired t tests provided moderate evidence in favor of H_0 of no change in connectivity strength ($BF_{10} < 0.26$). These results suggest that the observed gPPI changes are specific to the active wing-viewing task state and are not general consequences of VR exposure or passive viewing of the VR environment.

In summary, VR training induced wing-selective changes in functional connectivity with the right OTC_{wing}, reflected in increased connectivity with frontoparietal high-level somatosensory and motor associate regions when perceiving wing images. These effects were not observed when participants watched egocentric VR flying videos, indicating a functional-semantic embodiment of wings rather than generalized attentional or exposure effects.

Associations between neural and behavioral changes

We examined whether the neural changes observed in the univariate, MVPA, and gPPI analyses were associated with behavioral changes, including objective performance (change in hit rate for the ring navigation task) and subjective sense of agency ratings for the wings. All neural and behavioral indices were computed as post-versus pre-VR differences, with baseline conditions controlled for (see STAR Methods). Spearman's correlations were calculated across these indices (Figure S5). Non-significant correlations between these indices were observed (all $|\rho_{[23]}| < .31$, $p > .05$), indicating that VR-induced neural and behavioral changes were not linearly detectable within the current study design. Potential explanations are discussed further in the Discussion.

DISCUSSION

Advances in technology increasingly enable humans to transcend evolutionary constraints, such as moving at unprecedented speeds or even becoming airborne. VR pushes these boundaries further by allowing users to experience embodying artificial non-human body effectors that are never biologically present, such as wings. Understanding how the brain adapts to such experiences offers a valuable window into its capacity to process information beyond innate sensorimotor congruence. Here, by comparing neural responses to wing images before and after VR training, in which virtual wings are controlled by upper-limb movements, we identified three key changes in the OTC (Figure 5). First, this region exhibited bilaterally heightened univariate responses to wings. Second, the right OTC's multi-voxel patterns for wings became more similar to those representing upper limbs. Third, the right OTC's functional connectivity with frontoparietal high-level somatosensory and motor associate regions—critical for integrating motor, somatosensory, and proprioceptive information[43,44]—was selectively enhanced during wing viewing. These findings collectively suggest that the OTC dynamically incorporates atypical effectors into its representational architecture for body parts when they acquire specific functions, even in the absence of direct evolutionary or sensorimotor precedent.

The observed VR-flying-induced change was localized to OTC clusters, in the ventral and anterior portion of the classic LOTC or EBA, regions implicated in body processing[5,7] and multisensory integration.[45] The right OTC exhibited more robust representational and connectivity change than the left (as shown in the laterality and asymmetry analyses), which mirrors the preferential engagement of the right OTC in representing (non-hand) body parts.[6] Such VR-training-induced activity strength and changes in representational patterns for virtual wings add to the

Summary

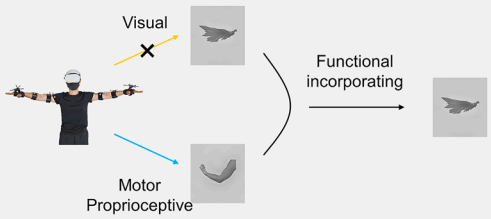

Neural changes	Result in OTC
univariate strength	↑ **wing-selective** activation strength; bilateral OTC
representational pattern	↑ **wing-upper-limb-selective** similarity; right OTC
functional connectivity	↑ **wing-selective** connectivity to high-level somatosensory/motor associate regions; right OTC

Figure 5. Study summary
Schematic integration of neural changes supporting functional-semantic embodiment of wings following VR training.

cumulative evidence challenging classic accounts of the OTC as a purely visual region.[9,10] While prior studies have identified nonvisual factors that modulate OTC representations, they are compatible both with an abstract functional-semantic account, as often assumed, and with a more parsimonious explanation rooted in intrinsic sensorimotor relations.[13,46] Crucially, such intrinsic sensorimotor relation factors cannot explain current findings, as the wing-upper-limb association was functionally constructed during VR training rather than evolutionarily innate. Instead, these results show that the OTC integrates wings moving closer to body representational space, which transcend low-level sensorimotor congruence. Our paradigm also rules out the simpler alternative that visual familiarity alone drove the neural changes: the effects generalized to untrained wing exemplars and specifically involved functional alignment between wings and upper limbs in representational similarity.

It is important to note that we are not suggesting that the wing has already become part of the canonical body representation. Indeed, both before and after training, wings do not reach the limb-level of activation in the EBA (see Figure S1), and wings' neural representations remain numerically more similar to object categories such as animal tails or tools in OTC regions than to limbs (see Figure S3). We merely report that their neural response profiles became significantly more similar to those of body parts (increased activation amplitude or enhanced representational similarity to upper limbs) as a result of VR training.

Intriguingly, previous studies have shown that tool or prosthetic expertise sharpens object category boundaries—making prosthetics less similar to either tools or body parts in the LOTC[23,25]—whereas our VR flying training enhances the representational similarity between wings and biological limbs in multi-voxel patterns. This divergence underscores the importance of multimodal congruence in shaping OTC representational structures. For tools and prosthetics, the use of an external object is directly driven by upper limb actions, maintaining simultaneous visual and motor processing of all these elements and reinforcing their distinct identities; for VR training, limb movement and visibility are decoupled. Upper-limb movements now drive wing movements that result in the dynamic change of scenes. The semantic interpretation of wings as potential biological effectors (and the absence of the upper-limb visual feedback) allows the VR training to align wings with upper limbs, increasing their neural representational similarity.

Beyond the primary effects of wings, other changes associated with the VR training warrant discussion. First, in the univariate analysis, lower faces showed an increased activation post-training (Figure 2). This effect was not accompanied by corresponding representational changes in the MVPA. It may reflect a transfer of low-level visual features (e.g., curvature) shared with wings, which are known to be encoded in OTC responses.[47,48] Second, in the MVPA results, there was a trend toward increased similarity between upper limbs and chairs, as well as between upper limbs and axes. This pattern suggests a potential "compression" effect, whereby the enhanced wing representation compresses the representational space for related categories.[38] These speculations are post-hoc and cannot explain the full range of results in a coherent manner, given inconsistencies across analyses, ROIs, and conditions. These results, however, highlight secondary effects that merit further investigation with targeted experimental designs.

Notably, we observed increased wing-selective gPPI connectivity between the right OTC and high-level somatosensory and motor associate regions following our VR training, with non-significant changes in connectivity to effector-specific S1/M1 upper-limb areas. These higher-level regions contain neuronal populations that form visuo-tactile receptive fields representing

the peripersonal space.[49,50] These receptive fields are crucial for the multisensory integration that supports the sense of ownership of body effectors, especially the upper limbs.[51–54] These regions are also known to share intrinsic functional connectivity with the OTC, as established in the literature.[17,18] Our gPPI results indicate that VR training specifically enhanced this pre-existing functional communication pathway during the viewing of wings.

Our findings offer insights into how VR modulates neural representations. VR exposure often induces transient, stimulus-specific adaptation (e.g., changes in scene-selective cortex during visuospatial processing).[55] The present study extends these prior reports by demonstrating that a targeted training protocol can elicit specific changes through functional-semantic processes. Such results highlight the potential of VR to drive widespread neural changes by updating neural semantic representations, which is consistent with clinical VR paradigms where functional equivalence (e.g., treating a virtual limb as one's own) drives therapeutic plasticity in amputees.[56]

By decoupling evolutionary constraints from sensorimotor experience, VR reveals the capacity of the OTC to dynamically incorporate non-human effectors into body representations. This neural change is governed not by mere visual or motor exposure but by the functional-semantic properties of the effector. Our findings extend the understanding of embodiment as a hierarchical process in which abstract, functional coding in the OTC interacts with frontoparietal networks to reconcile atypical multimodal congruence with existing body representations.

Limitations of the study

One notable limitation of our study concerns the investigation of the brain-behavior relationship. We attempted to examine the link between the neural change indices (univariate, MVPA, and gPPI changes from pre- to post-VR) and behavioral modulations across VR sessions. Despite some correlational trends (e.g., SoA with neural indices; see Figure S5), none reached statistical significance. This null result may be attributed to two factors: first, the experimental design featured a higher sampling density for behavior (four sessions) than for neural measures (two time points), potentially constraining the ability to detect within-subject neural-behavioral coupling over time; second, while our sample size (n = 25) provided sufficient power to detect robust group-level changes, it may be underpowered to capture fine-grained linear relationships, which typically require larger samples.[57,58] Future studies with larger cohorts and more temporally aligned neural-behavioral sampling are warranted to accurately map the correspondence between behavioral and functional changes in the brain.

RESOURCE AVAILABILITY

Lead contact

Requests for further information and resources should be directed to and will be fulfilled by the lead contact, Yanchao Bi (ybi@pku.edu.cn).

Materials availability

The lower face stimuli in this study were adapted from a previous study.[59] Images of other conditions were obtained from an in-house collection. The stimulus set is available from the lead contact upon request.

Data and code availability

- Source data for all figures and tables in this paper have been deposited at OSF (osf.io/yu298/; see key resources table) and are publicly available as of the date of publication.
- All original codes have been deposited at OSF (osf.io/yu298/; see key resources table) and are publicly available as of the date of publication.
- Any additional information required to reanalyze the data reported in this paper is available from the lead contact upon request.

ACKNOWLEDGMENTS

This work was supported by the National Natural Science Foundation of China (NSFC; 32595491 to Y.B.), the Brain Science and Brain-like Intelligence Technology-National Science and Technology Major Project (2021ZD0204100 [2021ZD0204104] to Y.B.; 2021ZD0202600 to K.W.), the NSFC (32471099 and 62061136001 to K.W.; 32171052 to X.W.), and the Fundamental and Interdisciplinary Disciplines Breakthrough Plan of the Ministry of Education of China (JYB2025XDXM504 to Y.B.). We thank the National Center for Protein Sciences at Peking University in Beijing, China, for assistance with MRI data acquisition; Dr. Weiwei Men for help with optimizing the MRI sequence; and Chunfang Yan for help with MRI scanning and scheduling. We are grateful to Yuxuan Luo, Tianyu Hu, Dingchen Zhang, Xiaomin Mao, Tianyu Zheng, Shuyue Wang, and Haoyang Chen for help with data collection; Shuang Tian, Haojie Wen, and Ze Fu for suggestions in data analysis; and Huichao Yang, Shuyue Wang, and Haoyang Chen for feedback on earlier versions of the manuscript.

AUTHOR CONTRIBUTIONS

Z.X., conceptualization, data curation, formal analysis, investigation, visualization, methodology, validation, writing – original draft, and writing – review and editing; Y.C., data curation, formal analysis, investigation, methodology, writing – original draft, and writing – review and editing; X.W., funding acquisition, methodology, and writing – review and editing; K.W., conceptualization, funding acquisition, project administration, resources, supervision, and writing – review and editing; Y.B., conceptualization, funding acquisition, project administration, resources, supervision, writing – original draft, and writing – review and editing.

DECLARATION OF INTERESTS

The authors declare no competing interests.

DECLARATION OF GENERATIVE AI AND AI-ASSISTED TECHNOLOGIES IN THE WRITING PROCESS

Gemini 3 Flash was used for language polishing. The authors have critically reviewed the output and take full responsibility for the integrity and accuracy of the manuscript.

STAR★METHODS

Detailed methods are provided in the online version of this paper and include the following:

- KEY RESOURCES TABLE
- EXPERIMENTAL MODEL AND STUDY PARTICIPANT DETAILS
  - Human participants
- METHOD DETAILS
  - Experimental procedure overview
  - VR training regimen and behavioral measurement
  - Questionnaire
  - Procedures for task-fMRI experiments
- QUANTIFICATION AND STATISTICAL ANALYSIS
  - Behavioral performance analysis
  - Image acquisition
  - Image preprocessing
  - Generalized linear model

- ROI-level statistical analysis
- Univariate activation of wing images
- MVPA analyses
- Functional connectivity analyses
- Laterality computation
- Brain-behavior correlation analyses
- Univariate activation of body movements
- Brain visualization

SUPPLEMENTAL INFORMATION

Supplemental information can be found online at https://doi.org/10.1016/j.celrep.2026.117320.

Received: June 12, 2025
Revised: January 21, 2026
Accepted: April 8, 2026

REFERENCES

1. Barsalou, L.W. (2008). Grounded cognition. Annu. Rev. Psychol. *59*, 617–645.
2. Christ, O., and Reiner, M. (2014). Perspectives and possible applications of the rubber hand and virtual hand illusion in non-invasive rehabilitation: Technological improvements and their consequences. Neurosci. Biobehav. Rev. *44*, 33–44.
3. Slater, M., Spanlang, B., Sanchez-Vives, M.V., and Blanke, O. (2010). First person experience of body transfer in virtual reality. PLoS One *5*, e10564.
4. Ramirez, J.G., Vanhoyland, M., Ratan Murty, N.A., Decramer, T., Van Paesschen, W., Bracci, S., Op de Beeck, H., Kanwisher, N., Janssen, P., and Theys, T. (2024). Intracortical recordings reveal the neuronal selectivity for bodies and body parts in the human visual cortex. Proc. Natl. Acad. Sci. USA *121*, e2408871121.
5. Downing, P.E., Jiang, Y., Shuman, M., and Kanwisher, N. (2001). A cortical area selective for visual processing of the human body. Science *293*, 2470–2473.
6. Bracci, S., Ietswaart, M., Peelen, M.V., and Cavina-Pratesi, C. (2010). Dissociable neural responses to hands and non-hand body parts in human left extrastriate visual cortex. J. Neurophysiol. *103*, 3389–3397.
7. Orlov, T., Makin, T.R., and Zohary, E. (2010). Topographic representation of the human body in the occipitotemporal cortex. Neuron *68*, 586–600.
8. Op de Beeck, H.P., Brants, M., Baeck, A., and Wagemans, J. (2010). Distributed subordinate specificity for bodies, faces, and buildings in human ventral visual cortex. Neuroimage *49*, 3414–3425.
9. Bao, P., She, L., McGill, M., and Tsao, D.Y. (2020). A map of object space in primate inferotemporal cortex. Nature *583*, 103–108.
10. Konkle, T., and Alvarez, G.A. (2022). A self-supervised domain-general learning framework for human ventral stream representation. Nat. Commun. *13*, 491.
11. Striem-Amit, E., and Amedi, A. (2014). Visual cortex extrastriate body-selective area activation in congenitally blind people "seeing" by using sounds. Curr. Biol. *24*, 687–692.
12. Bracci, S., Cavina-Pratesi, C., Ietswaart, M., Caramazza, A., and Peelen, M.V. (2012). Closely overlapping responses to tools and hands in left lateral occipitotemporal cortex. J. Neurophysiol. *107*, 1443–1456.
13. Striem-Amit, E., Vannuscorps, G., and Caramazza, A. (2017). Sensorimotor-independent development of hands and tools selectivity in the visual cortex. Proc. Natl. Acad. Sci. USA *114*, 4787–4792.
14. Maravita, A., and Iriki, A. (2004). Tools for the body (schema). Trends Cogn. Sci. *8*, 79–86.
15. Bracci, S., Caramazza, A., and Peelen, M.V. (2015). Representational similarity of body parts in human occipitotemporal cortex. J. Neurosci. *35*, 12977–12985.
16. Wang, X., Peelen, M.V., Han, Z., He, C., Caramazza, A., and Bi, Y. (2015). How visual is the visual cortex? Comparing connectional and functional fingerprints between congenitally blind and sighted individuals. J. Neurosci. *35*, 12545–12559.
17. Zimmermann, M., Mars, R.B., De Lange, F.P., Toni, I., and Verhagen, L. (2018). Is the extrastriate body area part of the dorsal visuomotor stream? Brain Struct. Funct. *223*, 31–46.
18. Hutchison, R.M., Culham, J.C., Everling, S., Flanagan, J.R., and Gallivan, J.P. (2014). Distinct and distributed functional connectivity patterns across cortex reflect the domain-specific constraints of object, face, scene, body, and tool category-selective modules in the ventral visual pathway. Neuroimage *96*, 216–236.
19. Kubota, E., Yan, X., Tung, S., Fascendini, B., Tyagi, C., Duhameau, S., Ortiz, D., Grotheer, M., Natu, V.S., Keil, B., and Grill-Spector, K. (2025). White matter connections of human ventral temporal cortex are organized by cytoarchitecture, eccentricity and category-selectivity from birth. Nat. Hum. Behav. *9*, 955–970.
20. Hardwick, R.M., Caspers, S., Eickhoff, S.B., and Swinnen, S.P. (2018). Neural correlates of action: Comparing meta-analyses of imagery, observation, and execution. Neurosci. Biobehav. Rev. *94*, 31–44.
21. Caspers, S., Zilles, K., Laird, A.R., and Eickhoff, S.B. (2010). ALE meta-analysis of action observation and imitation in the human brain. Neuroimage *50*, 1148–1167.
22. Gomez, J., Barnett, M., and Grill-Spector, K. (2019). Extensive childhood experience with Pokémon suggests eccentricity drives organization of visual cortex. Nat. Hum. Behav. *3*, 611–624.
23. Schone, H.R., Maimon-Mor, R.O., Baker, C.I., and Makin, T.R. (2021). Expert tool users show increased differentiation between visual representations of hands and tools. J. Neurosci. *41*, 2980–2989.
24. van den Heiligenberg, F.M.Z., Orlov, T., Macdonald, S.N., Duff, E.P., Henderson Slater, D., Beckmann, C.F., Johansen-Berg, H., Culham, J.C., and Makin, T.R. (2018). Artificial limb representation in amputees. Brain *141*, 1422–1433.
25. Maimon-Mor, R.O., and Makin, T.R. (2020). Is an artificial limb embodied as a hand? Brain decoding in prosthetic limb users. PLoS Biol. *18*, e3000729.
26. Kong, G., He, K., and Wei, K. (2017). Sensorimotor experience in virtual reality enhances sense of agency associated with an avatar. Conscious. Cogn. *52*, 115–124.
27. Cai, Y., Yang, H., Wang, X., Xiong, Z., Kühn, S., Bi, Y., and Wei, K. (2024). Neural correlates of an illusionary sense of agency caused by virtual reality. Cereb. Cortex *34*, bhad547.
28. Julian, J.B., Fedorenko, E., Webster, J., and Kanwisher, N. (2012). An algorithmic method for functionally defining regions of interest in the ventral visual pathway. Neuroimage *60*, 2357–2364.
29. Wilke, M., and Lidzba, K. (2007). LI-tool: a new toolbox to assess lateralization in functional MR-data. J. Neurosci. Methods *163*, 128–136.
30. Wen, H., Song, Y., Liang, M., Zhang, P., Wang, X., and Bi, Y. (2023). Pulvinar Response Profiles and Connectivity Patterns to Object Domains. J. Neurosci. *43*, 812–826.
31. Seghier, M.L. (2008). Laterality index in functional MRI: methodological issues. Magn. Reson. Imaging *26*, 594–601.
32. Chao, L.L., Haxby, J.V., and Martin, A. (1999). Attribute-based neural substrates in temporal cortex for perceiving and knowing about objects. Nat. Neurosci. *2*, 913–919.
33. Peelen, M.V., Bracci, S., Lu, X., He, C., Caramazza, A., and Bi, Y. (2013). Tool selectivity in left occipitotemporal cortex develops without vision. J. Cogn. Neurosci. *25*, 1225–1234.
34. Lewis, J.W. (2006). Cortical networks related to human use of tools. Neuroscientist *12*, 211–231.
35. Yarkoni, T., Poldrack, R.A., Nichols, T.E., Van Essen, D.C., and Wager, T.D. (2011). Large-scale automated synthesis of human functional neuroimaging data. Nat. Methods *8*, 665–670.

36. Fan, S., Wang, X., Wang, X., Wei, T., and Bi, Y. (2021). Topography of visual features in the human ventral visual pathway. Neurosci. Bull. *37*, 1454–1468.

37. Kriegeskorte, N., Goebel, R., and Bandettini, P. (2006). Information-based functional brain mapping. Proc. Natl. Acad. Sci. USA *103*, 3863–3868.

38. Kieliba, P., Clode, D., Maimon-Mor, R.O., and Makin, T.R. (2021). Robotic hand augmentation drives changes in neural body representation. Sci. Robot. *6*, eabd7935.

39. McLaren, D.G., Ries, M.L., Xu, G., and Johnson, S.C. (2012). A generalized form of context-dependent psychophysiological interactions (gPPI): a comparison to standard approaches. Neuroimage *61*, 1277–1286.

40. Friston, K.J., Buechel, C., Fink, G.R., Morris, J., Rolls, E., and Dolan, R.J. (1997). Psychophysiological and modulatory interactions in neuroimaging. Neuroimage *6*, 218–229.

41. Song, X., Panych, L.P., and Chen, N.-K. (2016). Data-driven and predefined ROI-based quantification of long-term resting-state fMRI reproducibility. Brain Connect. *6*, 136–151.

42. Korhonen, O., Saarimäki, H., Glerean, E., Sams, M., and Saramäki, J. (2017). Consistency of regions of interest as nodes of fMRI functional brain networks. Netw. Neurosci. *1*, 254–274.

43. Gottlieb, J. (2007). From thought to action: the parietal cortex as a bridge between perception, action, and cognition. Neuron *53*, 9–16.

44. Rolfs, M., and Schweitzer, R. (2022). Coupling perception to action through incidental sensory consequences of motor behaviour. Nat. Rev. Psychol. *1*, 112–123.

45. Tsakiris, M. (2010). My body in the brain: a neurocognitive model of body-ownership. Neuropsychologia *48*, 703–712.

46. Vannuscorps, G., F Wurm, M., Striem-Amit, E., and Caramazza, A. (2019). Large-scale organization of the hand action observation network in individuals born without hands. Cereb. Cortex *29*, 3434–3444.

47. Long, B., Yu, C.-P., and Konkle, T. (2018). Mid-level visual features underlie the high-level categorical organization of the ventral stream. Proc. Natl. Acad. Sci. USA *115*, E9015–E9024.

48. Zachariou, V., Del Giacco, A.C., Ungerleider, L.G., and Yue, X. (2018). Bottom-up processing of curvilinear visual features is sufficient for animate/inanimate object categorization. J. Vis. *18*, 3.

49. Graziano, M.S., Cooke, D.F., and Taylor, C.S. (2000). Coding the location of the arm by sight. Science *290*, 1782–1786.

50. Graziano, M.S. (1999). Where is my arm? The relative role of vision and proprioception in the neuronal representation of limb position. Proc. Natl. Acad. Sci. *96*, 10418–10421.

51. Nilsson, M., and Kalckert, A. (2021). Region-of-interest analysis approaches in neuroimaging studies of body ownership: An activation likelihood estimation meta-analysis. Eur. J. Neurosci. *54*, 7974–7988.

52. Guterstam, A., Björnsdotter, M., Gentile, G., and Ehrsson, H.H. (2015). Posterior cingulate cortex integrates the senses of self-location and body ownership. Curr. Biol. *25*, 1416–1425.

53. Petkova, V.I., Björnsdotter, M., Gentile, G., Jonsson, T., Li, T.-Q., and Ehrsson, H.H. (2011). From part-to whole-body ownership in the multisensory brain. Curr. Biol. *21*, 1118–1122.

54. Gentile, G., Guterstam, A., Brozzoli, C., and Ehrsson, H.H. (2013). Disintegration of multisensory signals from the real hand reduces default limb self-attribution: an fMRI study. J. Neurosci. *33*, 13350–13366.

55. Kravitz, D.J., Saleem, K.S., Baker, C.I., and Mishkin, M. (2011). A new neural framework for visuospatial processing. Nat. Rev. Neurosci. *12*, 217–230.

56. Vassantachart, A.Y., Yeo, E., and Chau, B. (2022). Virtual and augmented reality-based treatments for phantom limb pain: a systematic review. Innov. Clin. Neurosci. *19*, 48–57.

57. Schönbrodt, F.D., and Perugini, M. (2013). At what sample size do correlations stabilize? J. Res. Pers. *47*, 609–612.

58. Cohen, J. (1992). A Power Primer. Psychol. Bull. *112*, 155–159.

59. Bai, L., Hui, M., Huang, Y., and Luo, Y. (2005). The Development of Native Chinese Affective Picture System-A pretest in 46 College Students. Chin. Ment. Health J. *19*, 719–722.

60. Whitfield-Gabrieli, S., and Nieto-Castanon, A. (2012). Conn: a functional connectivity toolbox for correlated and anticorrelated brain networks. Brain Connect. *2*, 125–141.

61. Willenbockel, V., Sadr, J., Fiset, D., Horne, G.O., Gosselin, F., and Tanaka, J.W. (2010). Controlling low-level image properties: the SHINE toolbox. Behav. Res. Methods *42*, 671–684.

62. Xia, M., Wang, J., and He, Y. (2013). BrainNet Viewer: a network visualization tool for human brain connectomics. PLoS One *8*, e68910.

63. Faul, F., Erdfelder, E., Buchner, A., and Lang, A.-G. (2009). Statistical power analyses using G* Power 3.1: Tests for correlation and regression analyses. Behav. Res. Methods *41*, 1149–1160.

64. Xiong, Z., Tian, Y., Wang, X., Wei, K., and Bi, Y. (2023). Gravity matters for the neural representations of action semantics. Cereb. Cortex *33*, 6862–6871.

65. Oldfield, R.C. (1971). The assessment and analysis of handedness: the Edinburgh inventory. Neuropsychologia *9*, 97–113.

66. Op de Beeck, H.P. (2010). Against hyperacuity in brain reading: spatial smoothing does not hurt multivariate fMRI analyses? Neuroimage *49*, 1943–1948.

67. Hendriks, M.H.A., Daniels, N., Pegado, F., and Op de Beeck, H.P. (2017). The effect of spatial smoothing on representational similarity in a simple motor paradigm. Front. Neurol. *8*, 222.

68. Gardumi, A., Ivanov, D., Hausfeld, L., Valente, G., Formisano, E., and Uludağ, K. (2016). The effect of spatial resolution on decoding accuracy in fMRI multivariate pattern analysis. Neuroimage *132*, 32–42.

69. Chang, C.-C., and Lin, C.-J. (2011). LIBSVM: a library for support vector machines. ACM Trans. Intell. Syst. Technol. *2*, 1–27.

70. Tzourio-Mazoyer, N., Landeau, B., Papathanassiou, D., Crivello, F., Etard, O., Delcroix, N., Mazoyer, B., and Joliot, M. (2002). Automated anatomical labeling of activations in SPM using a macroscopic anatomical parcellation of the MNI MRI single-subject brain. Neuroimage *15*, 273–289.

STAR★METHODS

KEY RESOURCES TABLE

REAGENT or RESOURCE	SOURCE	IDENTIFIER
Deposited data		
Behavioral data	This study	OSF: osf.io/yu298/
Neuroimaging data	This study	OSF: osf.io/yu298/
Custom analysis code	This study	OSF: osf.io/yu298/
Experimental models: Organisms/strains		
Human	N/A	N/A
Software and algorithms		
MATLAB	MathWorks	RRID: SCR_001622; https://www.mathworks.com
SPM12	Wellcome Center for Human Neuroimaging, UCL	RRID: SCR_007037; https://www.fil.ion.ucl.ac.uk/spm/software/spm12/
CONN functional connectivity toolbox	Whitfield-Gabrieli and Nieto-Castanon[60]	RRID: SCR_009550; https://web.conn-toolbox.org/
SHINE toolbox	Willenbockel et al.[61]	http://www.mapageweb.umontreal.ca/gosselif/SHINE/
E-prime	Psychology Software Tools	RRID: SCR_009567; https://www.pstnet.com/eprime.cfm/
JASP	The JASP Team	RRID: SCR_015823; https://jasp-stats.org
BrainNet Viewer	Xia et al.[62]	RRID: SCR_009446; https://www.nitrc.org/projects/bnv/
Unity	Unity Technologies	https://unity.com
Motive	OptiTrack	https://optitrack.com/software/motive
Other		
3 Tesla Trio MRI scanner	Siemens	N/A
Optitrack FLEX	OptiTrack	https://optitrack.com/cameras
Oculus Quest	Meta Platforms	https://www.meta.com/es/en/quest/products/quest-2/

EXPERIMENTAL MODEL AND STUDY PARTICIPANT DETAILS

Human participants

We recruited 25 (15 females; mean age ±SD = 22.41 ± 3.12 years, range = 18.6–34.3 years) East Asian Chinese male and female human participants for the current study. The sample size was determined through a power analysis using G*Power 3.1[63] for our behavioral measurements of VR training, i.e., a one-way repeated-measures ANOVA with one group and four measurements. The results from power analysis indicated that a sample size of $n = 24$ would be sufficient to detect a large effect size ($\alpha = 0.05$, power = 0.9, Cohen's $f > 0.4$) for the VR training. This estimate is also consistent with our previous fMRI studies on VR and/or sensorimotor training, which typically enrolled around 25 participants.[27,64]

This study employed a within-subject design and participants were not assigned to separate experimental groups, and all participants completed both the VR training and fMRI experiments. None of them reported a history of neurological or psychiatric diagnoses. They were right-handed, as determined by the Edinburgh Handedness Inventory,[65] had normal or corrected-to-normal vision, and all were native Mandarin Chinese speakers. Informed consent was obtained from all participants before the experiments. The study was approved by the Ethical Committee of the School of Psychological and Cognitive Sciences at Peking University in accordance with the Declaration of Helsinki (Ethics approval number: #2020-04-17).

METHOD DETAILS

Experimental procedure overview

Each participant underwent the following experimental procedure: pre-VR MRI scanning, VR training, and post-VR MRI scanning. Each pre- and post-VR scanning lasted approximately 75 min, during which the participants performed a series of tasks within an

MRI scanner. These tasks included a *semantic-judgment experiment*, a *picture-viewing experiment*, a *motor localizer experiment*, and a *video-viewing experiment*. The *semantic-judgment experiment* was designed to address questions unrelated to the current study and is not reported here.

Following the pre-VR scanning, the participants underwent a VR training regimen consisting of four sessions. Each session lasted approximately 30 min and was distributed over a span of seven days, except for one participant who completed the fourth VR training session on the ninth day after the pre-VR scanning. During the VR training sessions, participants wore a head-mounted display (HMD, Oculus Quest 2; https://www.meta.com/es/en/quest/products/quest-2/; 72 Hz refresh rate, 1832 × 1920 per eye rendering) along with six sets of reflective markers placed on their bilateral upper arms, lower arms, and hands (see Figure 1A). Their upper-limb movements were recorded from these markers using a motion capture system (OptiTrack FLEX V100; https://optitrack.com/cameras; 100 Hz sampling rate). The kinematic data were streamed synchronously to drive a virtual wing-flapping animation displayed in the HMD, allowing participants to control a pair of virtual wings in a series of gamified VR tasks (see VR Training regimen and behavioral measurement). Additionally, questionnaires investigating participants' subjective feelings of wing embodiment were administered after each training session (see Questionnaire).

Post-VR MRI scanning was performed within one hour of the final training session, with the exception of one participant who was scanned on the subsequent day.

VR training regimen and behavioral measurement

During the VR training sessions, the positions and orientations of participants' upper limbs were computed synchronously using Motive (2.3.1, OptiTrack control software; https://optitrack.com/software/motive) and streamed to the virtual wings in the VR environment (Unity 2020.3.21f1; Unity Technologies; https://unity.com). The motion of the virtual wings consistently matched participants' real upper-limb kinematics. By controlling the virtual wings to execute goal-directed movements, the VR training sessions aimed to facilitate participants' embodiment of the virtual wings.

Each VR session began with a familiarization phase that included a posture imitation task and an airball task, lasting approximately five minutes in total. In the posture imitation task, the outline of a wing posture was displayed on a virtual mirror before participants. The target posture in each trial was randomly selected from six possible postures, such as the T-pose, N-pose, and right-wing-up pose. The participants were required to replicate the presented posture with their virtual wings. Once they reproduced the posture, the next target would appear, and the process would continue until all eight trials (two repetitions for the T-pose and N-pose) were successfully completed. In the airball task, a virtual green ball appeared at random locations and speeds, moving toward the participants. They were instructed to deflect the ball using their wings for eight trials.

After the familiarization phase, participants took part in a flying training phase that lasted about 25 min. During this time, flapping the virtual wings downward or upward would generate upward lift or downward drag, respectively, in line with aerodynamics in the program. To ascend as quickly as possible, participants needed to fully extend their wings and flap vigorously during the downward stroke to create lift while contracting their wings during the upward stroke to reduce the air contact area and thus minimize drag. The flying training tasks included single flap, maximum-velocity flight, altitude maintenance, and ring navigation (see Figure 1A for illustrations). In the single flap task, participants performed one flap to reach the highest possible altitude. In the maximum-velocity flight task, they flapped continuously to ascend to a target height as rapidly as possible. In the altitude maintenance task, participants maintained their altitude within a predefined range for a fixed duration. In the ring navigation task, they controlled their altitude while flying forward to pass through as many rings as possible. The first three tasks each included at least six training trials, whereas the ring navigation task consisted of one trial.

Following the flying training phase, participants completed an additional ring navigation task as a test phase. The hit rate (percentage of successful ring passes) for this task was recorded as a measure of participants' performance in controlling the virtual wings. The positions of the rings remained consistent for all participants across all four training sessions.

Questionnaire

After each VR training session, participants completed a questionnaire assessing their sense of agency (SoA, the subjective experience of voluntary control). The SoA was measured using two items rated on a 7-point Likert scale (1 = strongly disagree, 7 = strongly agree):

"I felt as if I could control movements of the virtual wings."

"I felt as if the virtual wings' movements obeyed my will."

To account for task compliance and suggestibility effects, a control statement was included:

"It seemed as if the virtual wings had a will on their own."

The items included in the questionnaire were adopted from established neurophysiological studies on VR illusions.[26,27]

Procedures for task-fMRI experiments

Picture-viewing experiment

This experiment utilized a block-design paradigm encompassing eight conditions: upper limbs, lower limbs, and lower faces (representing human body effectors); axes and chairs (representing man-made manipulable and nonmanipulable objects); animal tails; VR-self wings (wing stimuli used in VR training); and bird wings that were not used in VR training. Each condition comprised two sets of

grayscale images (seven each, 400 × 400 pixels, visual angle: 8.2 ° × 8.2 °) on a gray background. The lower face images were acquired from neutral faces in the "Chinese Affective Picture System",[59] VR-self-wing images were generated from various angles and orientations within the VR program's modeling files, and other images were sourced from our in-house collections. Each image underwent manual adjustment to ensure uniformity in the mean pixel count across conditions, while luminance, Michelson contrast, and spatial frequency were standardized using the SHINE toolbox (http://www.mapageweb.umontreal.ca/gosselif/SHINE/).[61] Four runs were performed, each lasting 254 s. Each run commenced with a 10 s fixation period and ended with a 16 s fixation period. The eight conditions were randomized with a Latin square, and two randomized lists were combined, resulting in 16 task blocks, each lasting 12 s. Each task block presented eight images (one stimulus set plus one repeated image for one-back repetition detection task) for 800 ms in a randomized sequence, with a 700 ms fixation interval. Each run thus featured all 14 images from two sets for each condition and participants were asked to press a button when the same image appeared consecutively. One 12 s rest block (fixation only) was interposed following every four task blocks, i.e., two such rest blocks per run, to prevent habituation, reduce drift, and enhance the signal-to-noise ratio for the subsequent blocks. The sequence of sets was counterbalanced across runs, participants, and scanning sessions.

Video-viewing experiment

The experiment consisted of one run lasting 200 s. It began with a 10 s fixation period, followed by a first-person-perspective video of an example flight, and concluded with a 14 s fixation period. The video (1,024 × 576 pixels, visual angle: 20.7 ° × 11.7 °, 176 s) depicted a dynamically changing scene of flying at different altitudes in an artificial canyon, identical to the ring-flight task but with the ring invisible, which was filmed by one of the authors (Y.C.). The video content was identical across participants and scanning sessions.

Motor localizer experiment

This experiment utilized a block-design paradigm involving five action conditions corresponding to different body effectors: left and right upper limbs (fully flexing and extending all fingers), left and right lower limbs (tapping and flexing the feet at the ankle), and lower face (opening and closing the lips). The task consisted of one run lasting 254 s, which began with a 12 s silence, followed by 20 task blocks, and concluded with a 12 s silence. The five types of task blocks were divided into four groups, each presented in a random order, thereby creating a sequence of 20 task blocks that varied across subjects and scanning sessions. After every five task blocks, a 10 s rest block was interposed. Each task block began with a 2 s auditory cue corresponding to one of the body effectors (recorded by one of the authors [Z.X.], a native Mandarin speaker), followed by beeps paced at 1 Hz, prompting subjects to perform the corresponding action once. Each rest block began with a 2 s auditory cue followed by beeps paced at 1 Hz, during which subjects stayed still. Throughout the task, subjects kept their eyes closed.

Visual stimuli were presented using E-Prime software (E-Prime 2 for the *video-viewing experiment* and E-Prime 1 for other experiments; RRID: SCR_009567; https://www.pstnet.com/eprime.cfm/), with images or videos projected onto an LCD display and viewed through a mirror mounted on the head coil.

QUANTIFICATION AND STATISTICAL ANALYSIS

Behavioral performance analysis

To assess participants' performance in controlling the virtual wings, we analyzed data from the ring navigation task during the test phase. The raw data were resampled to a standardized rate of 30 Hz to account for random fluctuations in the motion tracking system's refresh rate. We subsequently computed the flight altitude at each ring passage to determine the hit rate. For the statements in the questionnaire, we computed the average score of the two SoA statements for SoA measurements, and used the score of the control item for task compliance and suggestibility effects measurements. Within-subject repeated-measures analyses of variance (ANOVA) were used to measure behavioral changes.

Image acquisition

All functional and structural MRI data were collected using a Siemens Prisma 3T scanner with a 64-channel phase-array head coil at the Center for MRI Research, Peking University. The participants lay supine with their heads fixed with foam pads to minimize head motion. For structural MRI data, high-resolution 3D T1-weighted anatomical images were acquired before and after VR training separately via the magnetization-prepared rapid-acquisition gradient-echo sequence (192 sagittal slices, phase encoding direction from anterior to posterior, repetition time [TR] = 2530 ms, echo time [TE] = 2.98 ms, flip angle [FA] = 7°, voxel size = 0.5 × 0.5 × 1 mm^3, and interpolated matrix size = 448 × 512). The functional data were acquired with a simultaneous multislice sequence (62 axial slices, phase encoding direction from posterior to anterior, TR = 2000 ms, TE = 30 ms, multiband factor = 2, FA = 90°, voxel size = 2 × 2 × 2 mm^3 with a gap of 0.3 mm, and matrix size = 112 × 112).

Image preprocessing

Using statistical parametric mapping software (SPM12; RRID: SCR_007037; https://www.fil.ion.ucl.ac.uk/spm12/) in MATLAB (Mathworks; RRID: SCR_001622), the following initial preprocessing steps were applied to all the functional data: (A) the first five volumes of each run for signal equilibrium were discarded; (B) slice timing correction and head motion correction were performed; (C) the images were spatially normalized to the Montreal Neurological Institute (MNI) space using unified segmentation, and

resampled into 2 mm isotropic voxels; and (D) the images were spatially smoothed using a 6 mm full-width at half-maximum (FWHM) Gaussian kernel for univariate analyses and functional connectivity (FC) analyses and a 2 mm FWHM Gaussian kernel for multi-voxel pattern analyses (MVPA) to maximize signal-to-noise ratio, as previous studies suggested.[66–68] Head motion for all participants remained within acceptable limits, with no motion exceeding 2 mm or 2°.

For FC analyses, the preprocessed data were further denoised using the CONN Toolbox (RRID: SCR_009550; https://web.conn-toolbox.org/).[60] This denoising process included regressing out (A) ten principal components from the white matter and cerebrospinal fluid (CSF) time series extracted from principal component analysis; (B) head motion-related artifacts by including six head motion parameters, six first-order derivatives, and 12 quadratic effects; and (C) task-related BOLD signals through bandpass filtering at 0.008 Hz to eliminate slow fluctuating signals, such as scanner drift. For generalized psychophysiological interaction (gPPI) analyses, the denoising step further included regressing out task predictors, session effects, and the rest effect during first-level generalized linear modeling (GLM).

Generalized linear model

Preprocessed functional data from the *picture-viewing experiment* were entered into the GLM using SPM. For univariate analyses, the GLM was built on all runs of the task and included regressors of each experimental condition (eight in total) as predictors of interest, along with the six head motion parameters. For MVPA, the GLM included every single block as a unique predictor of interest, resulting in 64 (eight conditions × two repetitions × four runs) predictors of interest. Six head motion parameters were also included as predictors of no interest. Each predictor was convolved with a canonical hemodynamic response function (HRF), and a high-pass-filter cutoff was set at 128 s. After model estimation, whole-brain beta maps were calculated for each regressor relative to rest periods, resulting in eight maps for univariate analyses and 64 for MVPA.

For the functional data from the motor localizer experiment, the GLM included regressors for each body effector's movement (five in total), plus one regressor corresponding to the rest blocks as predictors of interest, along with six head motion parameters, each convolved with a canonical HRF. A high-pass filter cutoff was set at 128 s. After model estimation, whole-brain beta maps were calculated for each body effector's movement (five) relative to rest periods for further analyses.

ROI-level statistical analysis

In primary ROI analyses, statistical significance was defined using repeated measures ANOVA or paired *t* tests (two-tailed). Significance levels are indicated in figures as follows: ***$p < .001$, **$p < .01$, and *$p < .05$. All error bars in figures represent standard error of the mean (SEM).

For key ROI-level analyses where frequentist statistics failed to reject the null hypothesis, we conducted complementary Bayesian analyses to quantify the evidence in favor of the null hypotheses (e.g., H_0: no interaction or difference between conditions). These were performed using JASP software (The JASP Team; RRID: SCR_015823; https://jasp-stats.org) with default Cauchy priors ($r = .707$). This approach was specifically employed to distinguish between inconclusive results and those providing positive evidence for the absence of a certain effect. The definition of ROIs are presented below.

Occipitotemporal regions

These regions included classic LOTC or EBA, as well as functionally defined OTC regions showing wing-selective functional profile changes (OTC_{wing}).

The former classic regions were used as ROIs for univariate analyses and MVPA, which include: (A) anatomically defined LOTC ($LOTC_{anat}$), based on the Harvard-Oxford atlas (probability >.25, including the inferior division of lateral occipital cortex and the temporooccipital part of middle temporal gyrus; 2897 and 3196 voxels for left and right LOTC, respectively); (B) *Neurosynth*-defined EBA ($EBA_{neurosynth}$). Neurosynth (https://www.neurosynth.org/)[35] is an online platform for large-scale, automated meta-analyses based on the fMRI database of 14,371 studies. We searched the term "body", which revealed 552 studies tagged with it. The association test map was thresholded at false-discovery rate of .01, from which we generated spherical ROIs (radius = 8 mm, 257 voxels) centered at the two largest clusters representing the right (peak MNI coordinates [50–70 0]) and left EBA (peak MNI coordinates [–46 –72 6]). We also applied EBA parcels defined in Julian et al.[28] to compare the location of clusters derived in whole-brain analyses.

The latter region was used as seed region for connectivity analyses, which were functionally defined as regions showing significant univariate response changes of wings following VR training (measured in fMRI univariate interactions of VR training [post vs. pre] × object type (wing vs. non-wing) at the group-level threshold of voxel-level $p < .001$, cluster-level FWE corrected $p < .05$, see the "Univariate activation of wing images" section). We generated spherical seeds (radius = 4 mm, 33 voxels) centered at the peak of the OTC_{wing} to ensure maximum signal homogeneity within seed regions.[41,42]

Somatosensory and motor regions

These regions included primary somatosensory and motor (S1/M1) upper-limb regions and high-level somatosensory and motor associate regions. S1/M1 upper-limb regions were functionally defined by contrasting the movement of the upper limb with the average movement of the lower limb and lower face at the ipsilateral site of the body, merging the activation strength across pre- and post-fMRI scanning sessions (from the *motor localizer experiment* at the group-level threshold of voxel-level FWE corrected $p < .05$, see below). High-level somatosensory and motor associate regions were generated as spherical (radius = 8 mm, 257 voxels) regions on the basis of the peak MNI coordinates of a conjunction result of motor imagery, action observation, and movement execution from a previous meta-analysis.[20] These regions included the bilateral supplementary motor area (bi-SMA, MNI coordinates

[−2 8 54]), left and right dorsal premotor cortex (l- and r-PMd, MNI coordinates [−34 −10 58] and [36 −8 60]), left and right ventral premotor cortex (l- and r-PMv, MNI coordinates [−56 8 28] and [54 10 30]), and left and right inferior parietal lobe (l- and r-IPL, MNI coordinates [−42 −32 48] and [44 −34 56]).

Univariate activation of wing images

To test whether brain responses to wing images were modulated by VR training, VR training × object type interactions were calculated in the *picture-viewing experiment*.

Whole-brain univariate analyses

Individual beta-weight images were produced following model estimation in the GLM for the contrasts designed to measure wing activation. Since two types of wing stimuli (namely, VR-self-wing and bird-wing) were included in our experiment, we averaged the beta values of the two conditions to represent the neural response to wings and subtracted the values from the average of other conditions. These beta-weighted maps were then subjected to group-level random-effects (RFX) analyses. Paired *t* tests contrasting post- and pre-VR sessions (for both directions) were conducted to measure activation contrasts modulated by VR experience.

ROI-level univariate analyses

We also carried out ROI-level analysis. For each classic LOTC and EBA ROI (i.e., $LOTC_{anat}$ and $EBA_{neurosynth}$), we extracted the averaged beta values of wing and non-wing conditions from each participant. These values were then submitted to a within-subject repeated-measures ANOVA (factors: VR training × object type). When comparing different types of wings, the VR training (post, pre) × object type (VR-self-wing, bird-wing) interaction was adopted.

MVPA analyses

ROI-level MVPA

We performed MVPA within OTC regions using beta values extracted for each condition from pre- and post-VR sessions. A Support Vector Machine (SVM) in the LIBSVM library[69] with split-half cross-validation classified all pairs of conditions across all run combinations. Representational similarities (100% − accuracy) were submitted to repeated-measures ANOVA (factors: VR training [post, pre] × object pair type [wing-upper-limb, wing-others]) to assess changes in "wing-upper-limb" similarity. We also tested whether the effects were driven by changes in upper limb representations, using direct comparisons (paired *t* tests) of "upper-limb−other" similarity, and by VR training (post, pre) × object pair type (wing-upper-limb, upper-limb−others) interaction. When comparing between different types of wings, we computed a wing-upper-limb similarity index for each wing type by subtracting the averaged wing-other conditions similarity from wing-upper-limb similarity, yielding two types of indices (VR-self-wing, bird-wing). These values were then tested in VR training (post, pre) × wing type (VR-self-wing-index, bird-wing-index) interaction effects.

Whole-brain searchlight analyses

We further conducted whole-brain searchlight MVPA[37] restricted to the cortical gray matter regions in the AAL atlas (#1−#90).[70] For each voxel, a spherical searchlight (radius = 8 mm, 257 voxels) was centered on that voxel, and the multi-voxel patterns within the sphere were extracted for each condition. Using the same SVM classifier and cross-validation scheme as in the ROI-level analyses, we computed classification accuracies for each object pair. We then derived the contrast of "wing-upper-limb vs. wing-other" similarity and assigned the resulting value to the center voxel. The contrast maps were spatially smoothed (6 mm FWHM) and submitted to group-level paired *t* tests comparing post- and pre-VR sessions.

Functional connectivity analyses

Generalized psychophysiological interaction analyses

PPI is a type of task-based functional connectivity analysis that identifies voxels and/or ROIs whose BOLD time series are correlated with that of a seed region under a specific psychological condition.[39] It describes task-state network-level activities beyond intrinsic connectivity.[40] Unlike classic PPI analysis, which includes certain contrasts as regressors, the gPPI method convolves the BOLD time series for each condition with the canonical HRF to create psychological regressors for each condition separately. In the subject-level analyses, after preprocessing the data, we extracted the BOLD time series from the OTC_{wing} seeds in the *picture-viewing task* for each subject and condition via CONN toolbox.[60] We applied a seed-to-voxel approach to determine the psychophysiological interaction strength between the seed region's BOLD time series and each task condition, resulting in eight Fisher-*z*-transformed *r* stat maps for each subject at each scanning session. ROI-level gPPI analyses were conducted by extracting the mean *r* values of all voxels in each ROI from the whole-brain gPPI maps. Repeated-measures ANOVA with factors VR training (post, pre) and object (wing, non-wing), or VR training (post, pre) and object (VR-self-wing, bird-wing) was conducted, and the interaction effects were used to assess connectivity changes. We also compared wing and non-wing conditions against zero in one-sample *t* tests, to better characterize the observed interaction. Three-way repeated-measures ANOVA with factors hemisphere (left, right), VR training (post, pre), and object (wing, non-wing) was conducted to assess hemispheric differences.

Task-state functional connectivity analyses

To test whether the regions showing strong PPI modulation might also exhibit VR-general change in connectivity, ROI-level FC was conducted between OTC_{wing} seeds and high-level somatosensory and motor associate regions. Specifically, we extracted the preprocessed BOLD time series from the OTC_{wing} seeds in the *video-viewing experiment* at the pre- and post-VR sessions and

Please cite this article in press as: Xiong et al., Virtual flying experience changes neural responses to seeing wings, Cell Reports (2026), https://doi.org/10.1016/j.celrep.2026.117320

computed the seed-to-voxel Pearson's correlation to assess the connectivity between the seed region and the rest of the brain, resulting in one *r* stat map for each subject at each scanning session. We then Fisher-*z* transformed the maps, and extracted the mean *r* values in high-level somatosensory and motor associate regions from the whole-brain FC maps. Paired *t* tests were performed between the pre- and post-VR scanning sessions to assess task-state connectivity changes.

Laterality computation

We computed the laterality index (*LI*) of univariate and MVPA changes in the $LOTC_{anat}$ mask using the LI toolbox.[29] The group-level *t* maps (in the direction of post vs. pre for whole-brain univariate analysis and/or whole-brain searchlight MVPA) were used to compute *LI* curves using a bootstrapping method (n = 10,000) with the following options: $LOTC_{anat}$ mask or the entire occipital lobe (implemented in the LI toolbox), no exclusive masking, and the default bootstrapping parameters. This method involved the calculation of 20 equally sized thresholds from 0 to the maximum statistical value. At each threshold, 100 bootstrapped samples were taken from the left and right anatomical OTC (200 in total). All 10,000 possible *LI* combinations (100 samples on the left $\times$ 100 samples on the right) were then calculated from these samples in surviving voxels using the formula [(L − R)/(L + R)]. Only the central 50% of the data were kept to exclude statistical outliers. A weighted mean *LI* was then calculated for each image, with all *LI*s weighted by their corresponding thresholds. The mean weighted *LI* index ranged from −1 to 1, with −1 indicating complete right lateralization and 1 indicating complete left lateralization. We adopted a stringent threshold that considered values between −.2 and .2 as bilateral.[30,31]

Brain-behavior correlation analyses

The aim of the brain-behavior correlation analyses was to examine whether individual differences in neural changes across participants were associated with behavioral improvements and/or changes in the sense of agency. Three types of neural change indices were defined in the OTC_{wing}, using the average non-wing conditions or non-wing-upper-limb condition pairs as baselines: (A) the univariate neural change index, representing the relative activation change from wings to non-wing conditions, calculated as ([post wing − post non-wing] − [pre wing − pre non-wing]); (B) the MVPA change index, reflecting the relative change in similarity (100% − classification accuracy) between the wing-upper-limb pair and the wing-other pair, calculated as ([post wing-upper-limb − post wing-other] − [pre wing-upper-limb − pre wing-other]); and (C) the gPPI change index, calculated similarly as ([post wing − post non-wing] − [pre wing − pre non-wing]). Note that the gPPI change index was computed based on the functional connectivity between the right OTC_{wing} spherical seed and the high-level somatosensory and motor associate regions. Two behavioral measures were used to capture VR training effects: (A) the change in hit rate in the ring task ([4th hit rate − 1st hit rate]), and (B) the change in explicitly rated sense of agency to the wings ([4th SoA − 4th control item] − [1st SoA − 1st control item]). Only the first and last behavioral sessions were included to match the temporal proximity of the pre- and post-VR fMRI scanning sessions. Spearman's correlation was used to test each pair of neural and behavioral indices for significant associations.

Univariate activation of body movements

To functionally localize upper-limb-specific S1/M1 areas, we contrasted the beta-weighted maps of upper-limb movements to the average of lower limb and lower face movements on the ipsilateral side of the body for each participant for pre- and post-VR fMRI data in the *motor localizer experiment*. We averaged the map across scanning sessions, which resulted in two contrast maps. These maps were submitted to group-level RFX analyses (one-sample *t* tests against zero) with voxel-level FWE correction at $p < .05$ across cortical regions, yielding the left and right upper-limb-specific S1/M1.

Brain visualization

The ROI illustration and whole-brain results are projected onto the MNI brain surface using BrainNet Viewer (RRID: SCR_009446; https://www.nitrc.org/projects/bnv/).[62]